A donor: hole-transport layer alloy for high-efficiency and stable binary organic solar cells with promoted hole collection and suppressed recombination

Experimental section

Materials:PM6, L8-BO and PDNIT-F3N were purchased from Solarmers Materials Inc. Zinc oxide (ZnO) nanoparticles were purchased from Avantama AG (Stäfa, Switzerland). SDS and all solvents were purchased from Sigma-Aldrich and used as received.

Donor NP synthesis and solution preparation: PM6 10 mg were dissolved in 1 mL chloroform and stirred at 40℃ for 1 hour. Then the solution was added to 10mL 10mg/mL SDS and the mixed solution was stirred for 1 hour at 1500 rpm. The formed micro-emulsion dispersion was ultrasonicated using a SCIENTZ-IID ultrasonic finger (250watt, 5 min) in a ice-water bath. Used Amicon® ultra-15 centrifuge filter (cutoff 30K) to remove the excess surfactant from the particle solution. The dispersion was place into the filter and centrifuged at 4000rpm for 10 min. The retentate was raised to 15 mL with water and centrifuged again. This process was repeated for 4 times. The retentate was filtered by a 0.45μm filter and diluted to 14mg/mL before mixing. The PM6 NPs ink with the same concentration as that of PEDOT:PSS (CLEVIOS TM P VP Al 4083) was added into PEDOT:PSS at different volume ratios (varying from 0.2% to 20%, v/v) and stirred for 30 min..

Solar cells fabrication and characterization: The ITO glass was firstly cleaned with acetone and isopropyl alcohol in an ultrasonic bath for 10 min each. For the conventional solar cell devices with the structure of ITO/PM6:PEDOT:PSS/Active

layer/PDNIT-F3N/Ag, the ITO substrates were coated with 30 nm of the mixed solution of PEDOT:PSS and PM6 NP by spin-coating at 5000 rpm and annealed at 160℃ for 15 min. The active layer PM6:L8-BO solution was dissolved by chloroform with polymer concentration of 7.5mg/mL(D:A=1:1.2,0.25% DIM) was spin-coated on HTL at 3400 rpm and annealed at 80℃ for 5 min. After active layer deposition, a 0.5mg/mL methanol solution of PDNIT-F3N was spin-coated at 2000 rpm for 35s in nitrogen atmosphere. For the inverted solar cells with a structure of ITO/ZnO/active layer/PM6:PEDOT:PSS/Ag, 30 nm ZnO (Avantama N−10) was firstly doctor bladed on the ITO substrate and annealed at 85◦C in air. After the active layer deposition, a isopropanol-diluted PM6:PEDOT:PSS ink (water:IPA = 1:3, v/v) was doctor-bladed with the substrate temperature kept at 65^{o} C. Then, the substrate was annealed at 110^{o} C for 5min in the glovebox, followed by thermal evaporation of 100 nm silver through a shadow mask with a 0.04 cm^2 active area opening under a vacuum of approximately 2×10^{-5}mbar. The current-voltage characteristics of the solar cells were measured under AM 1.5 G irradiation on a Newport solar simulator (Taiwan, China). The light source was calibrated with a silicon reference cell. All cells were tested under an inert atmosphere. EQEs were measured using an Enlitech QE-S EQE system (Taiwan, China) that was equipped with a standard Si diode. Then IQE were determined following the equation: IQE = EQE/(1 – Reflection). Monochromatic light was generated from a Newport 300 W lamp source. The photo-stability of the solar cells was performed under continuous 1 sun illumination from a LED light (wavelength range from 400 nm to 800 nm) in a home-built chamber filled with N_2.

Single carrier devices were fabricated and the dark J-V characteristics measured and analyzed in the SCL regime following the references. The structure of hole-only devices was glass/ITO/PM6:PEDOT:PSS(30 nm)/active layer/MoO_x(8 nm)/Ag(100 nm). The structure of electron-only devices was glass/ITO/ZnO(30 nm)/active layer/PDNIT-F3N(15 nm)/Ag(100 nm). The reported mobility data are average values

over 15 devices of each sample for a range of thickness. The SCLC curves can be fit to the Mott–Gurney relation for SCLC: [1]

$$J_{SCL} = \frac{9}{8}\varepsilon_0\varepsilon_r\mu\frac{V_{in}^2}{L^3}exp\left(\frac{0.89\beta}{L^{0.5}}V_{in}^{0.5}\right) \quad (1)$$

where J_{SCL} is the current density, $\varepsilon_0\varepsilon_r$ is the dielectric permittivity, μ is the carrier mobility, L is the film device, and β is the field activation factor.[2]

TPC, TPV, Photo-CELIV, CE, impedance and capacitance–voltage (C–V) measurements are measured by Paios setup from FLUXiM AG. The built-in potential (V_{bi}) from the C-V measurement can be calculated using the equation:[3]

$$\frac{1}{C^2} = \frac{2(V_{bi} - V)}{A^2 e\varepsilon_0\varepsilon_r N_t} \quad (2)$$

where C is the value of capacitance, V is the voltage applied in the devices, A is the device area, e is the element charge, ε_0 and ε_r are the vacuum permittivity and relative dielectric constant, and Nt is the trap density. Here, ε_r is determined by the capacitance value at a frequency (1 kHz) and V= 0 V in dark conditions according to the formula:[4]

$$C = \varepsilon_0\varepsilon_r\frac{A}{d} \quad (3)$$

where d is the thickness of the photoactive layer.

FTPS-EQE and EL-EQE measurements: FTPS-EQE was measured using a integrated system (PECT-600, Enlitech), where the photocurrent was amplified and modulated by a lock-in instrument. EL-EQE measurements were performed by applying external voltage/current sources through the devices (REPS-Pro, Enlitech). All of the devices

were prepared for EL-EQE measurements according to the optimal device fabrication conditions. EL-EQE measurements were carried out from 0 to 1.8 V.

Characterizations: Particle size and distribution were determined by dynamic light scattering (DLS) using a Malvern Zetasizer Nano ZS90 from Malven Panalytical (Malvern, UK). UV/Vis absorption, transmittance and reflectance spectra were measured using an UV-Vis-NIR spectrometer (Lambda 1050, from Perkin Elmer, Waltham, MA, USA). SEM results were obtained from the field emission scanning electron microscopy (FESEM) GeminiSEM 300 (Carl Zeiss Microscopy Ltd., Jena, Germany). AFM measurements were performed by Cypher S from Oxford Instruments Asylum Research, Inc. in contact mode. UPS experiments was performed on the Thermo Scientific XPS Escalab Xi+ using He I as the excitation source and its source energy was 21.21 eV. DSC measurements were taken with DSC 30 under nitrogen. The temperature ranged from 0 to 300℃ with a heating and cooling rate of 10 ℃/ min within 2 recycles. The NP solutions drop-casted on clean glass substrates, and dried in a vacuum oven at 60 °C for 48 h and under vacuum overnight. Contact angle measurements were carried out by an Attention Theta Flex meter, using water and diiodomethane by sessile drop analysis in open ambient atmosphere.

Time-of-flight secondary ion mass spectrometry: TOF-SIMS was performed using a TOF-SIMS instrument (ION TOF TOF-SIMS V), where a 10 keV Ar^+ cluster ion source was used for sputtering and a 25 keV Bi^{3+} pulsed primary ion beam was used for the analysis. The area of analysis was 150 × 150 μm^2.

Film-depth-dependent light absorption: Film-depth-dependent light absorption spectra were acquired by an in-situ spectrometer (PU100, Shaanxi Puguang Weishi Co. Ltd.) (Shaanxi, China) equipped with a soft plasma-ion source. The power-supply for generating the soft ionic source was 100 W 39with an input oxygen pressure ~10 Pa. The film surface was incrementally etched by the soft ion source, without damage to the materials underneath the surface, which was in situ monitored by a spectrometer.

From the evolution of the spectra and the Beer–Lambert's Law, film-depth-dependent absorption spectra were extracted. The exciton generation contour is numerically simulated upon inputting sub-layer absorption spectra into a modified optical transfer-matrix approach. The detailed experimental and numerical method are available elsewhere.[5,6]

The exciton formation of FLAS measurement is expressed by absorption coefficient. The absorption coefficient can be obtained according to

$$\alpha = 4\pi k/\lambda \quad (2)$$

$$I \approx I_0 e^{-\alpha(\lambda)d} \quad (3)$$

$$A(\lambda) = \lg(I_0/I) = -\lg(e^{-4\pi kd/\lambda}) \quad (4)$$

The real part (n) of complex index of refraction is set to be 2 for clarity, while the imaginary part (k) of complex refraction is from absorption coefficient (α) and absorbance (A). λ and d are wavelength and film thickness. k is related to film-depth. The detailed model is illustrated in elsewhere.[7]

Grazing-incidence wide-angle X-ray scattering: GIWAXS was measured at 13A beam line of National Synchrotron Radiation Research Center (NSRRC, Taiwan). All samples for GIWAXS were radiated at 12 keV X-ray with an incident angle of 0.2°.

In-situ annealing light absorption spectra: The in-situ annealing light absorption spectra experiments were performed on a multi-spectrometer (TU-300, Shaanxi Puguang Weishi Co. Ltd.). The annealing temperature was from 25℃ to 150 ℃ and the annealing speed was 12.5℃ each minute.

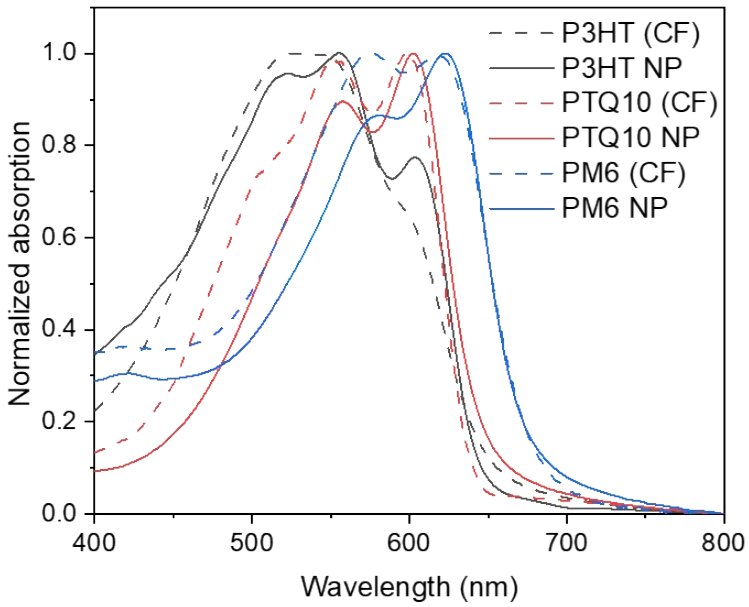

Figure S1. (a) UV-vis absorption spectra of P3HT, PTQ10 and PM6 films processed by chloroform and NPs.

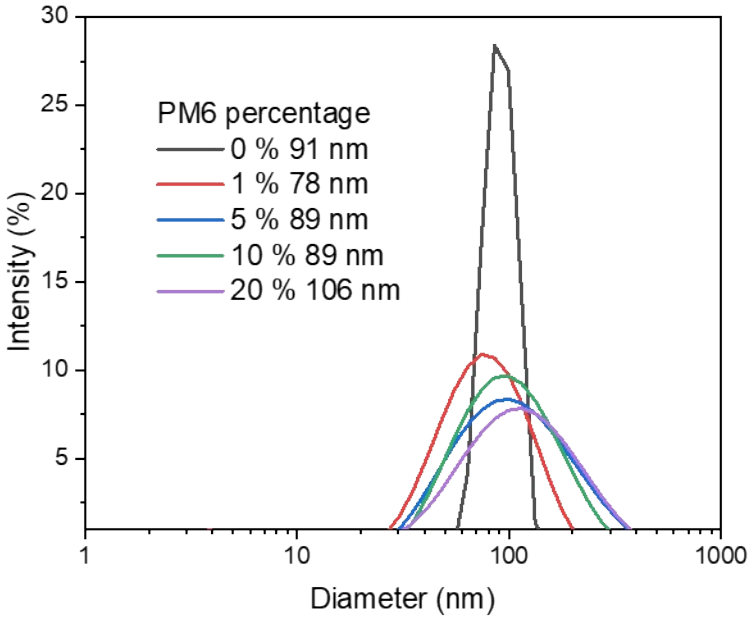

Figure S2. Particle size distribution of PM6:PEDOT:PSS dispersion from DLS measurements.

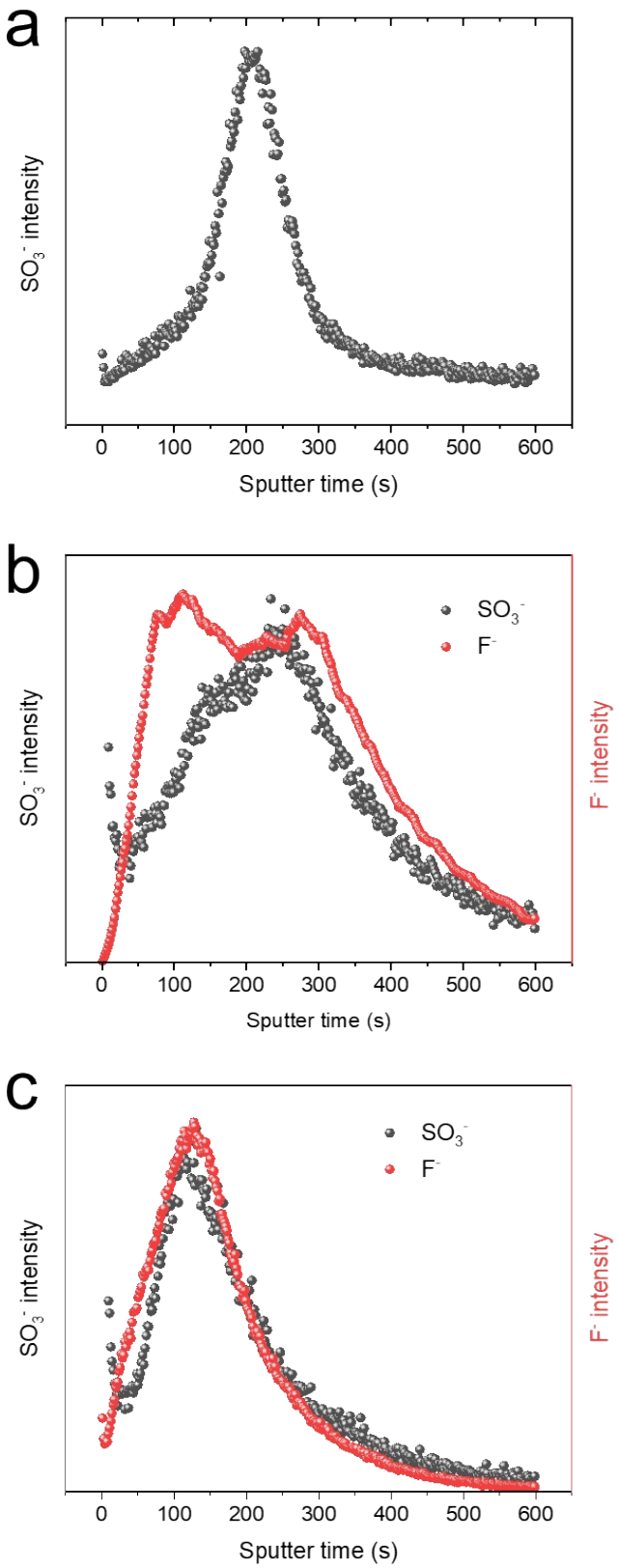

Figure S3. TOF-SIMS of (a) pure PEDOT:PSS, (b) as casted PM6 (20%):PEDOT:PSS film and (c) annealed of PM6:PEDOT:PSS film.

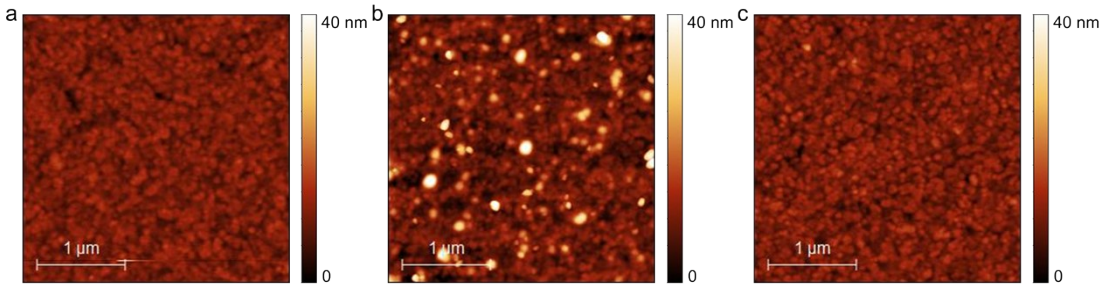

Figure S4. AFM images of (a) PEDOT:PSS, as casted PM6 (20%):PEDOT:PSS (b) before and (c) after thermal annealing.

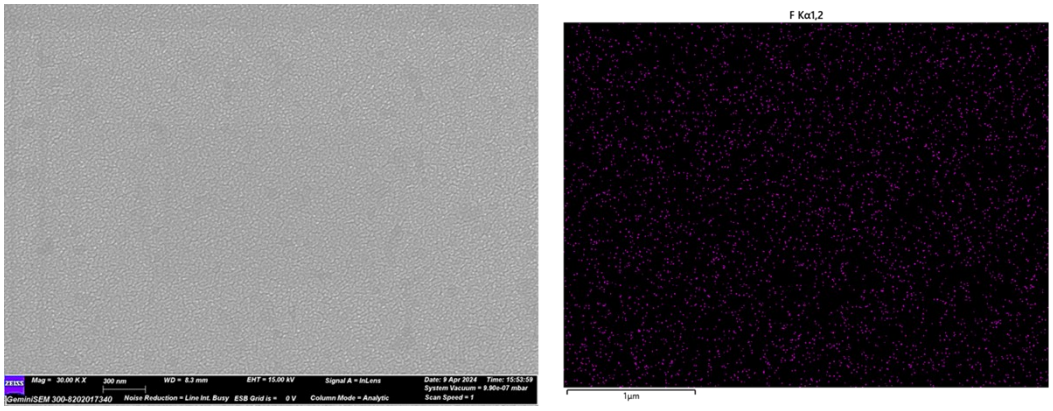

Figure S5. SEM of PM6:PEDOT:PSS surface (left) and its corresponding EDS mapping at the fluorine atom (right).

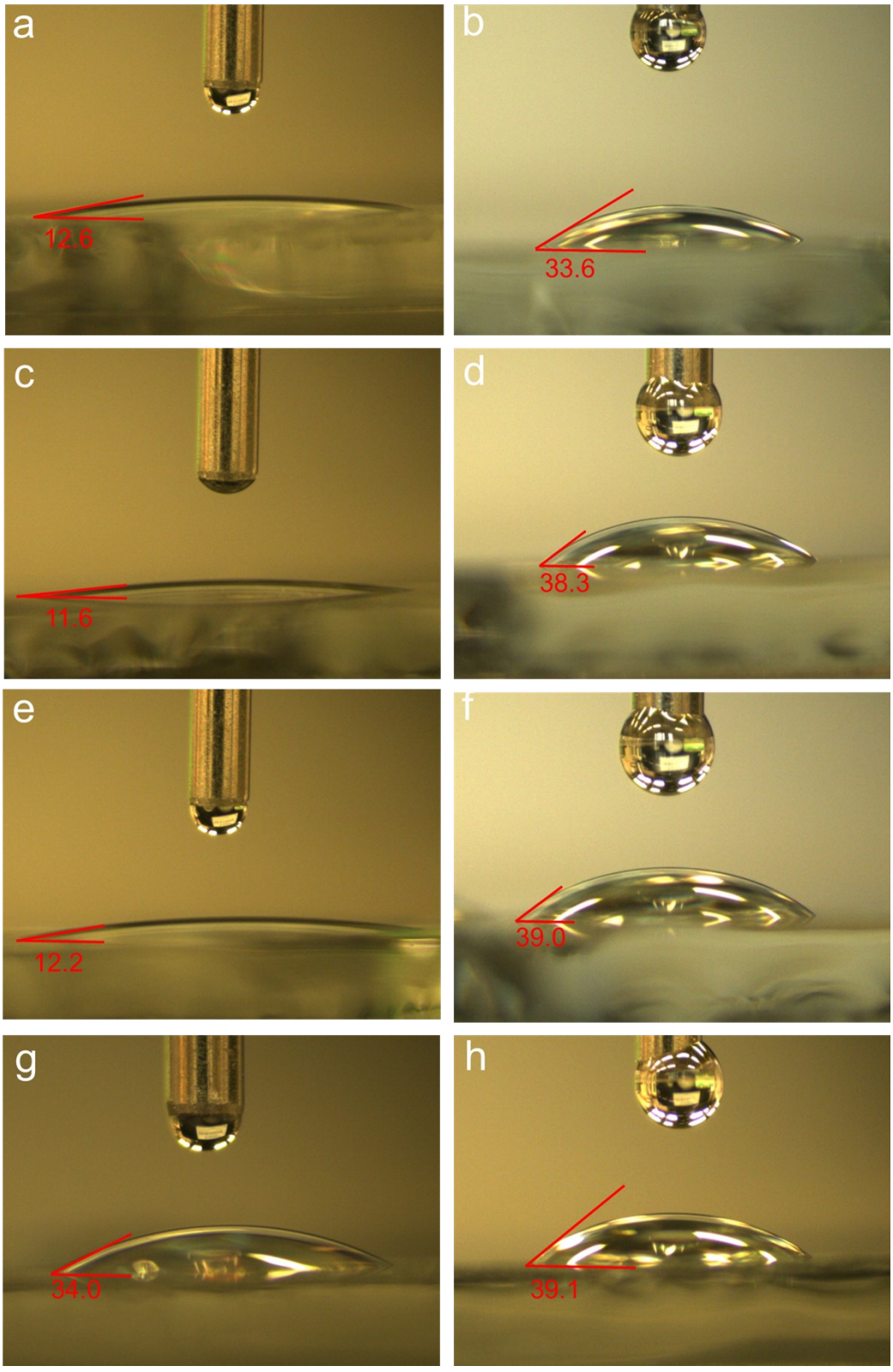

Figure S6. Contact angle images (a,c,e,g) of water and (b,d,f,h) of CH_2I_2 on top of (a,b) pure PEDOT:PSS, (c,d) PM6 (5%): PEDOT:PSS, (e,f) PM6 (10%): PEDOT:PSS and (g,h) PM6 (20%): PEDOT:PSS films, respectively.

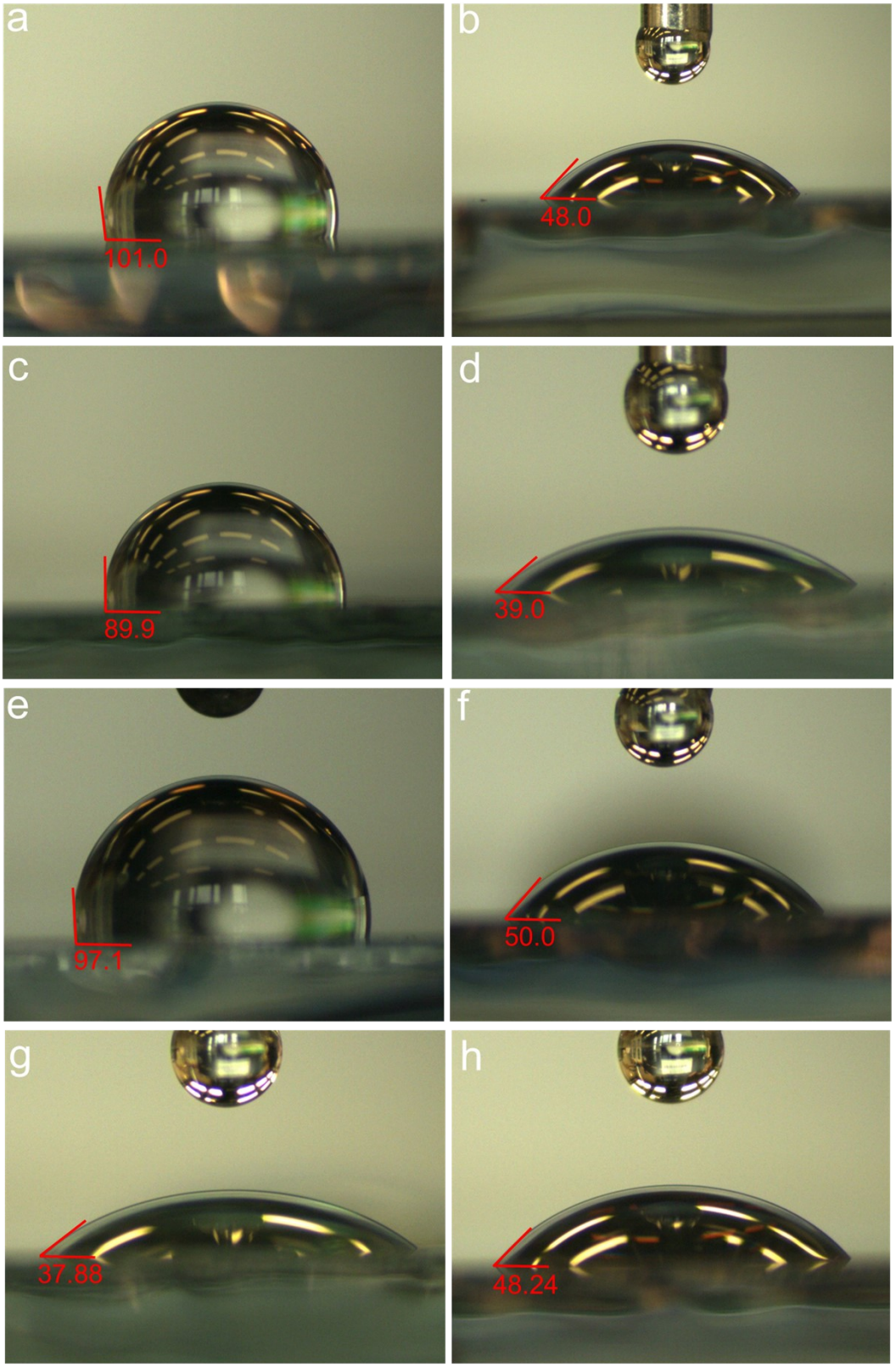

Figure S7. Contact angle images (a,c,e,g) of water and (b,d,f,h) of CH_2I_2 on top of se(a,b) pure PM6, (c,d) pure L8-BO, (e,f) PM6:L8-BO and (g,h) PM6 NP films, respectively.

Table S1. Contact angle results and surface energy values calculated according to Owens, Wendt, Rabel and Kaelble (OWRK) method.

Material	Water contact Angle	DIM contact Angle	Surface energy (mN/m)
PEDOT:PSS	12.6	33.6	76.32
PM6 (5 %):PEDOT:PSS	11.6	38.3	75.64
PM6 (10 %):PEDOT:PSS	12.2	39.0	75.37
PM6 (20 %):PEDOT:PSS	34.0	39.1	66.96
PM6	101.0	48.0	35.46
PM6 NP	37.9	48.2	62.69
L8-BO	89.9	39.0	41.02
PM6:L8-BO	97.1	50.0	34.70

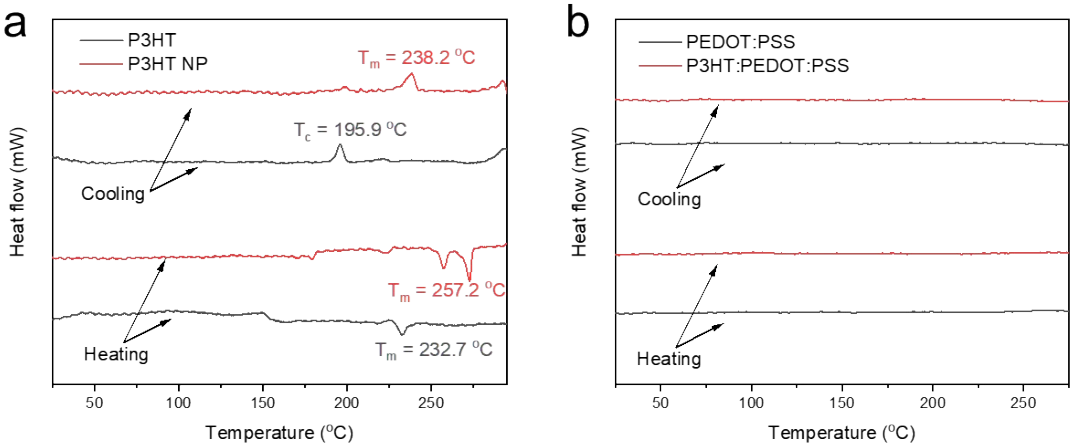

Figure S8. DSC heating and cooling scans of (a) P3HT and (b) P3HT blended with PEDOT:PSS samples.

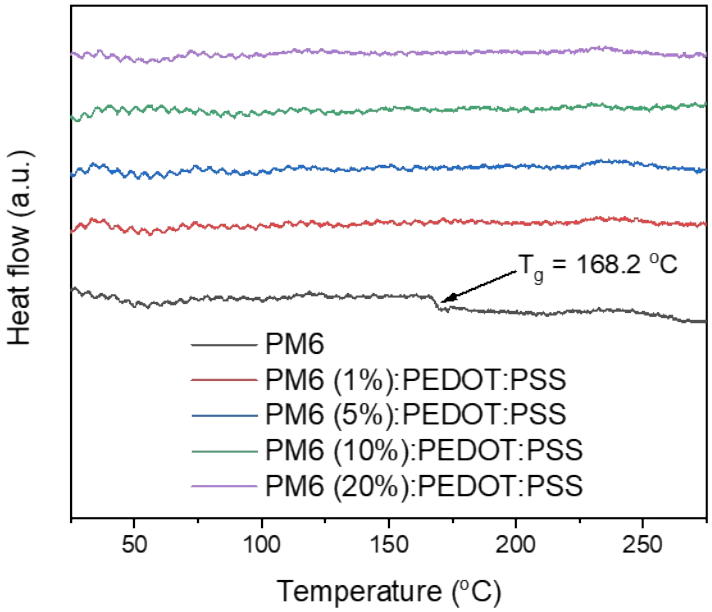

Figure S9. DSC cooling scans of PM6 and PM6 blended with PEDOT:PSS samples.

Table S2. The kinetic energy cutoff ($E_{cut-off}$), the Fermi levels (E_{Fermi}) and calculated work functions of different ITO/HTL films.

PM6 percentage	$E_{cut-off}$ (eV)	E_{Fermi} (eV)	Work function (eV)
0 %	6.29	-9.96	4.97
0.2 %	6.23	-9.99	5.00

1 %	6.19	-9.97	5.06
2 %	6.19	-9.95	5.08
5 %	6.16	-9.94	5.12
10 %	6.16	-9.97	5.10
20 %	6.22	-9.88	5.12
50 %	6.48	-9.41	5.33

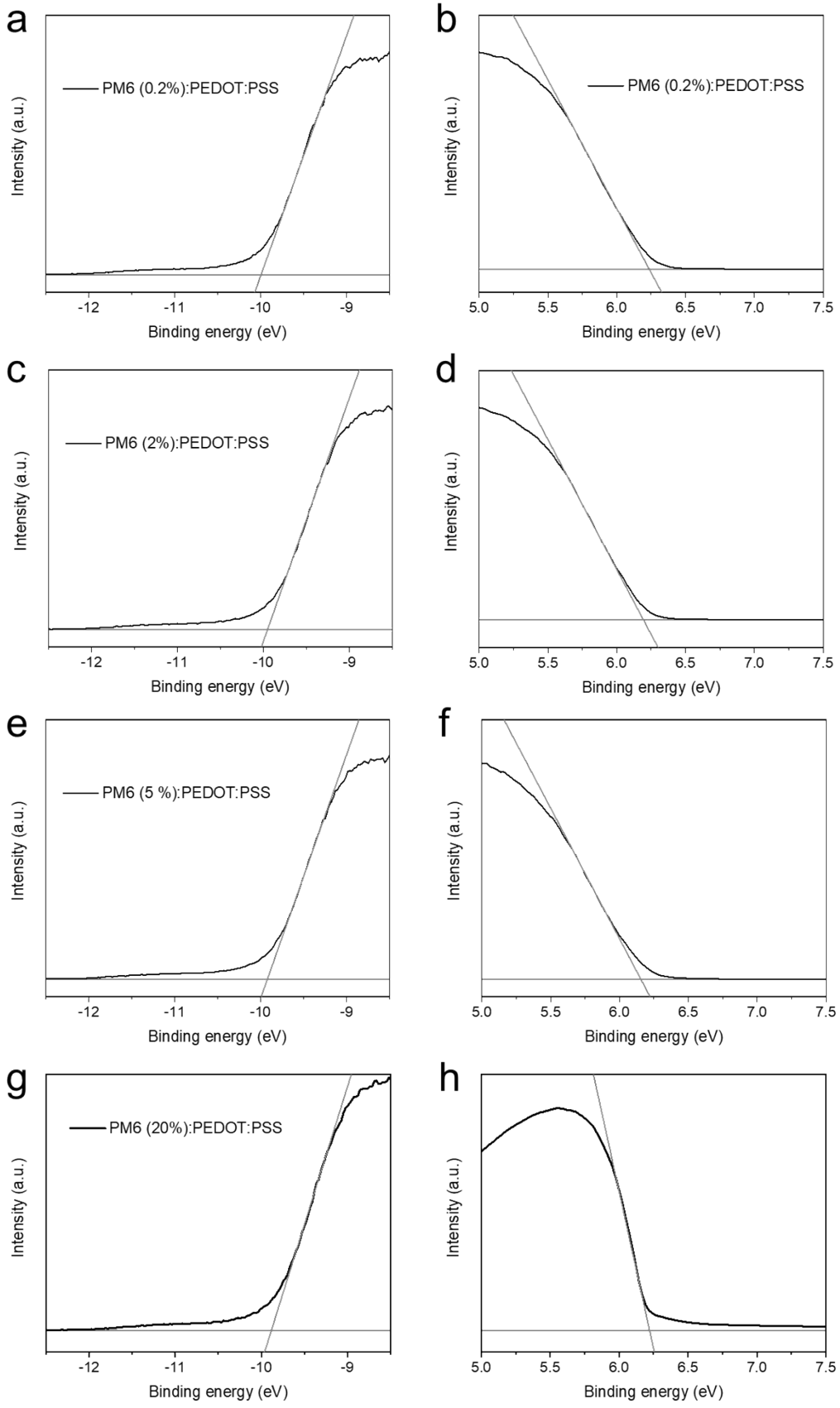

Figure S10. UPS spectra of PM6:PEDOT:PSS layer with (a,b) 0.2 %, (c,d) 2 %, (e.f) 5% and (g,h) 20% PM6.

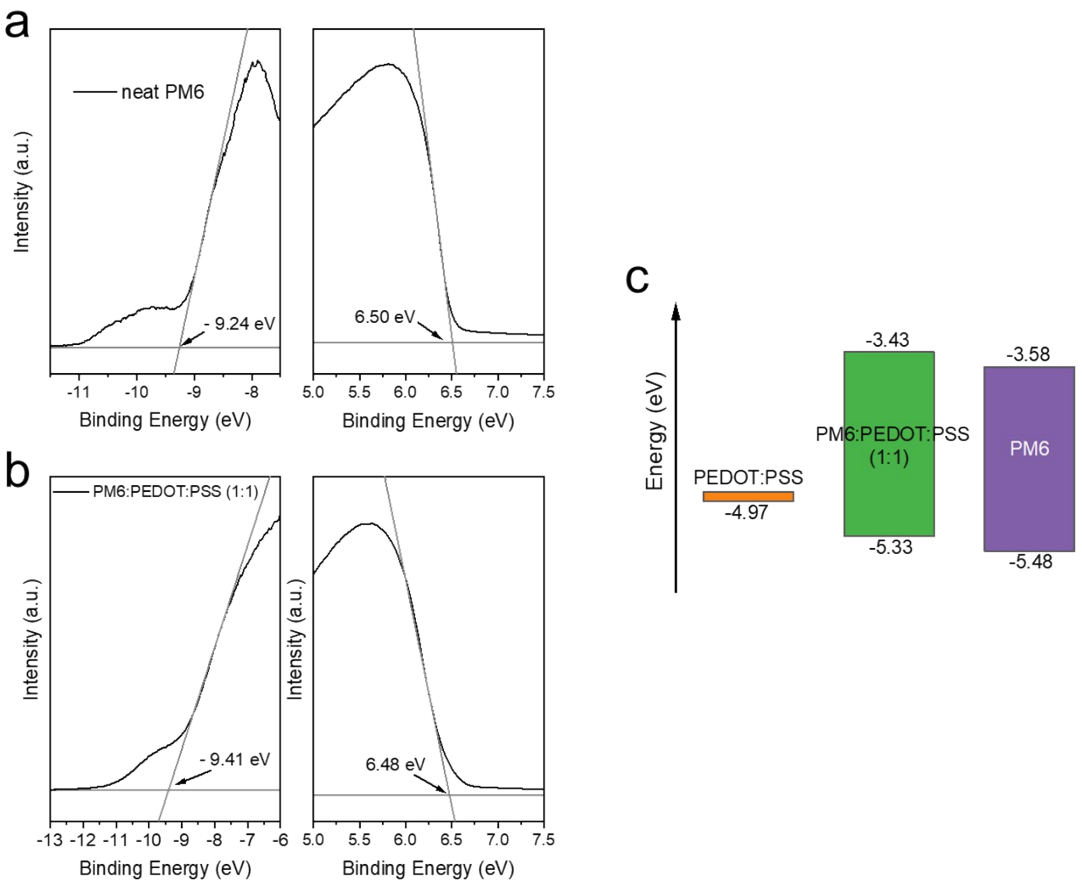

Figure S11. UPS spectra of (a) PM6 NP layer and (b) PM6 mixing with PEDOT:PSS (1:1) on ITO. (c) Energy level alignment of donor:HTL and PM6.

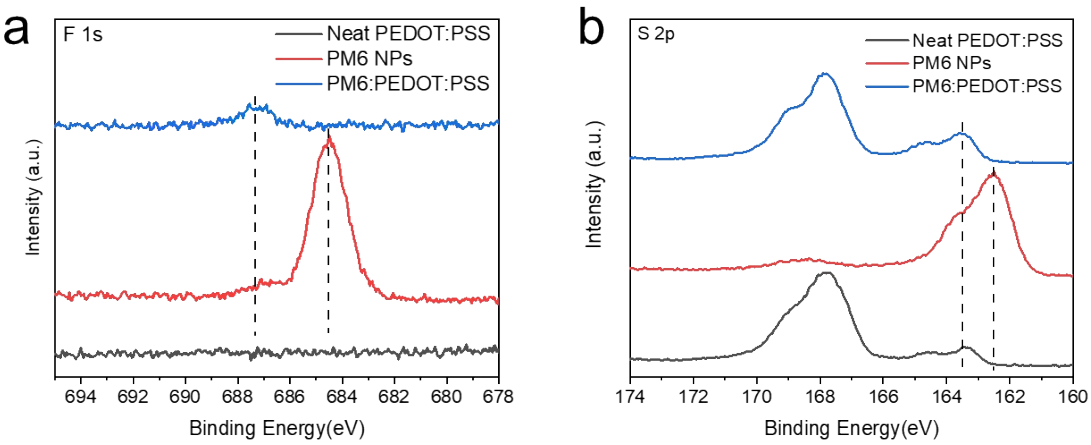

Figure S12. (a) F 1s and (b) S 2p XPS spectra of neat PEDOT:PSS, PM6 NPs and PM6 (10%):PEDOT:PSS.

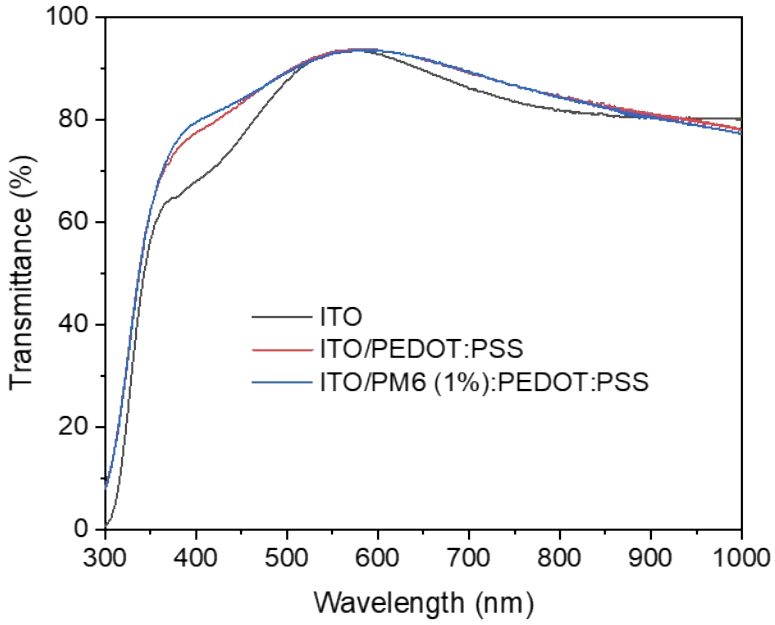

Figure S13. Transmittance spectra of PM6:PEDOT:PSS-treated ITO substrate.

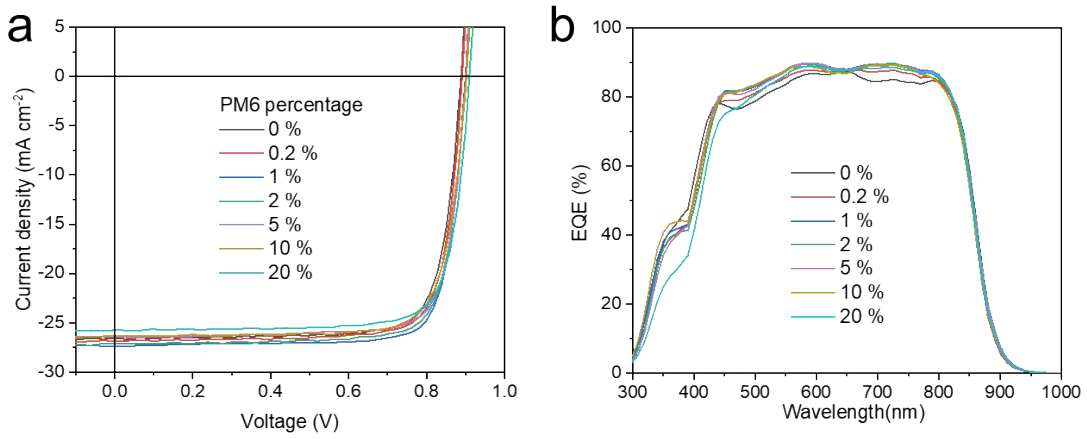

Figure S14. (a) J-V curves and (b) EQE spectra of PM6:PEDOT:PSS-based conventional devices with different PM6 percentages. Device architecture: ITO/HTL/active layer/PDNIT-F3N/Ag.

Table S3. Summary of photovoltaic parameters of PM6-L8-BO-based solar cells with different PM6 percentages in PEDOT:PSS.

PM6 percentage	V_{OC} (V)	J_{SC} (mA cm^{-2})	J_{SC}[a] (mA cm^{-2})	FF (%)	PCE[b] (%)
0 %	0.886	26.60	25.54	79.34	18.70 (18.45 ± 0.25)

0.2 %	0.889	26.88	25.65	79.57	19.00 (18.83 ± 0.19)
1 %	0.897	27.37	26.32	80.86	19.86 (19.57 ± 0.29)
2 %	0.898	27.14	26.12	79.77	19.44 (19.17 ± 0.27)
5 %	0.898	26.51	26.13	80.07	19.07 (18.90 ± 0.17)
10 %	0.900	26.36	25.97	78.35	18.59 (18.38 ± 0.21)
20 %	0.907	25.75	25.57	78.95	18.45 (18.22 ± 0.23)

天津市计量监督检测科学研究院电子仪表实验所

Tianjin Institute of Metrological Supervision and Testing Electronic & Instrumental Laboratory

检测报告

TEST REPORT

№：TDYF 字第 240013-WT　　共 4 页 第 4 页

检测内容：Test content	光伏电流-电压特性 *I-V* Characteristic		
序号 №	项目 Item	技术要求 Requirement	检测结果 Test result
1	光伏电流-电压特性 *I-V* Characteristic	—	见下表 As follows

测试时间 Date	2024.01.12							
测试条件 Condition	使用稳态 AAA 级太阳模拟器，在 AM1.5G，1000W/m²，25.0℃条件下测试 Sample was tested under the condition of AM1.5G, 1000W/m², 25.0°C with a steady-state class calibrated AAA solar simulator							
有效面积 Active area	0.0375cm² 备注：器件的有效面积是由带固定孔径的薄金属掩膜板量化 Remark: Designated area defined by thin metal aperture mask.							
样品编号 №	V_{oc} (V)	I_{sc} (mA)	J_{sc} (mA/cm²)	P_{max} (mW)	V_{Pmax} (V)	I_{Pmax} (mA)	*FF* (%)	η (%)
240013-1	0.885	1.021	27.23	0.724	0.750	0.966	80.16	19.32

测试程序 Test program settings		
	起始电压：Starting voltage:	-0.20V
	终止电压：Termination voltage:	+1.00V
	扫描间隔：Scan interval:	0.05V
	延迟时间：Delay time:	0.1s

I-V 曲线图 *I-V* curve

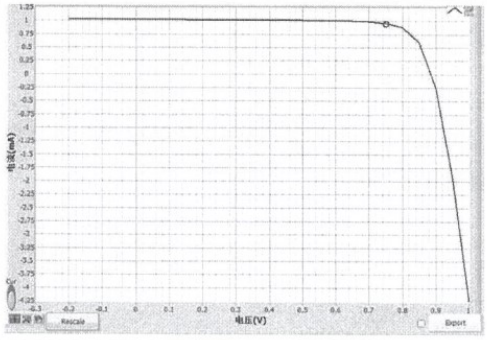

本报告结束 The end of the report

Figure S15. Certification report of PM6:L8-BO device from the Tianjin Institute of Metrological Supervision and Testing Electronic & Instrumental Laboratory.

Table S4. Classification of representative binary OSCs with record efficiency.

NO.	Year	System	PCE (measured)	PCE (certified)	Reference
1	2019	PM6:AQx-2	16.64	16.4	8
2	2020	PM6:Y6	17.3	17.1	9
3	2020	PM6:BTP-eC9	17.8	17.3	10
4	2021	PM6:Y6	17.11	16.77	11
5	2022	PM6:L8-BO	18.32	17.9	12
6	2022	PM6:BTP-eC9	18.5	18.2	13
7	2022	PM6:L8-BO	18.86	18.44	14
8	2023	D18:L8-BO	19.1	18.9	15
9	2023	PM6:L8-BO	18.85	18.7	16
10	2023	PM6:BTP-eC9	19.1	18.93	17
11	2023	PBQx-TF:eC9-2Cl	19.2	19	18
12	2023	PM6:BTP-eC9	19.3	18.93	19
13	2024	PM6:L8-BO	19.4	19.06	20
14	2024	D18:DT-C8Cl	19.4	18.9	21
15	2024	D18:Z19	19.2	18.8	22
16	2024	D18:AQx-2F	19.7	19.1	23
17	2024	PM6:L8-BO	19.86	19.32	This work

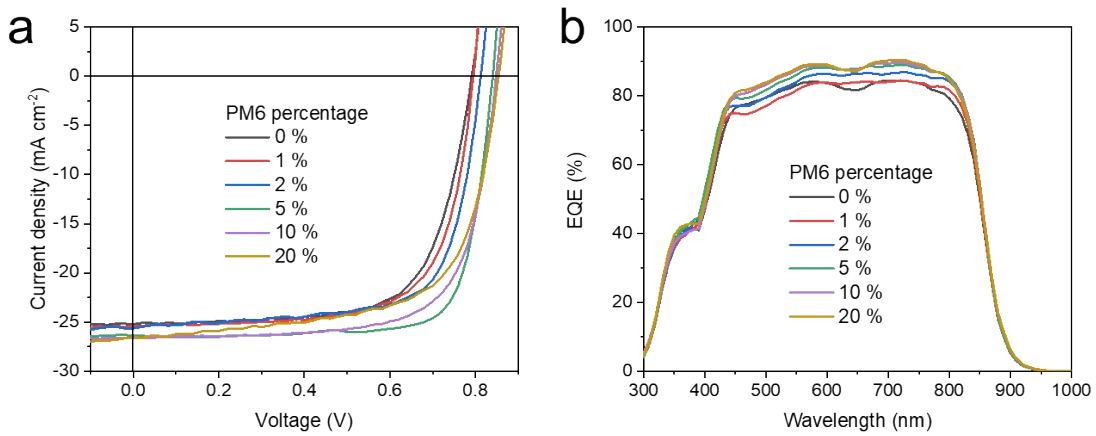

Figure S16. (a) J-V curves and (b) EQE spectra of PM6:PEDOT:PSS-based inverted devices with different PM6 percentages. Device architecture: ITO/ZnO/active layer/HTL/Ag.

Table S5. Summary of photovoltaic parameters of PM6-L8-BO-based inverted solar cells with different PM6 percentages in PEDOT:PSS.

PM6 percentage	V_{OC} (V)	J_{SC} (mA cm^{-2})	J_{SC} (mA cm^{-2})	FF (%)	PCE (%)
0 %	0.790	25.21	24.51	68.85	13.72 (13.45 ± 0.22)
1 %	0.793	25.41	24.58	69.40	13.98 (13.70 ± 0.28)
2 %	0.810	25.56	25.36	70.33	14.57 (14.47 ± 0.10)
5 %	0.839	26.35	25.86	77.74	17.17 (16.99 ± 0.27)
10 %	0.836	26.77	25.98	71.03	16.10 (15.99 ± 0.17)
20 %	0.852	26.81	26.09	65.25	14.91 (14.78 ± 0.13)

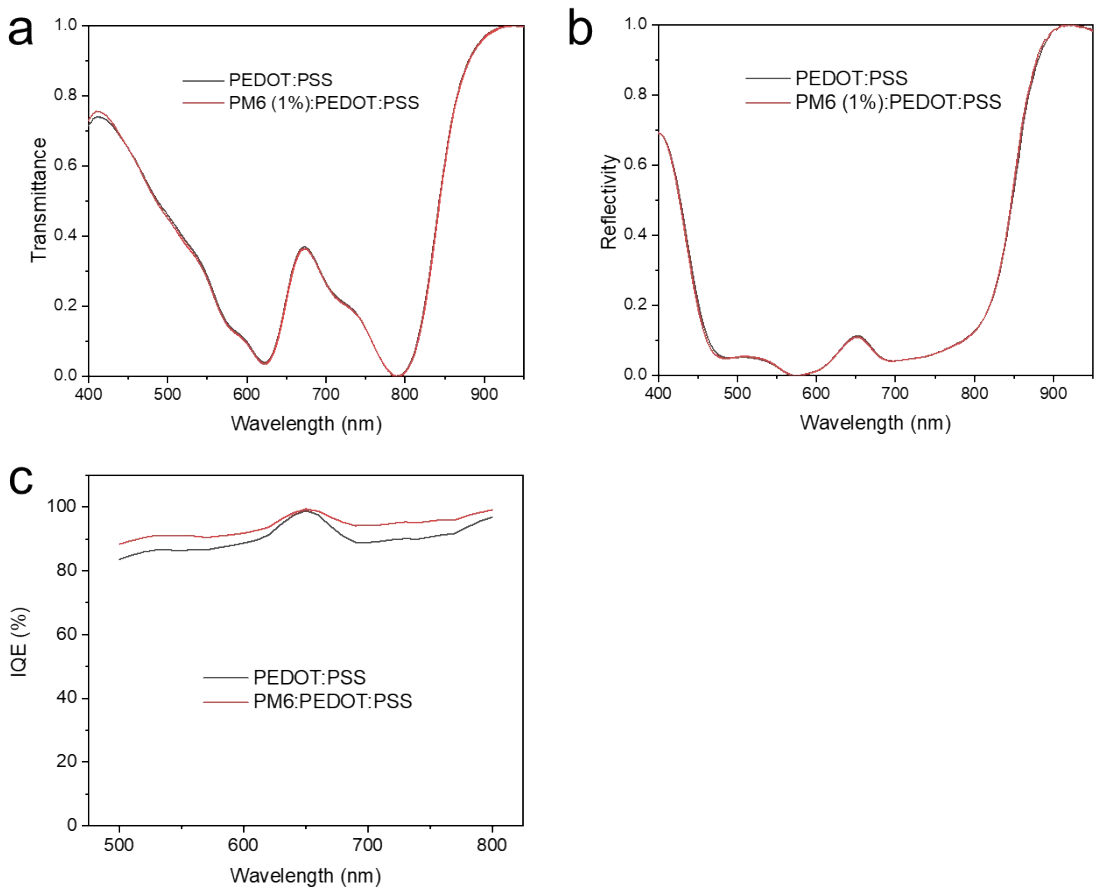

Figure S17. (a) Transmittance, (b) reflectivity and (c) IQE spectra of PM6 (1%): PEDOT:PSS-based conventional devices.

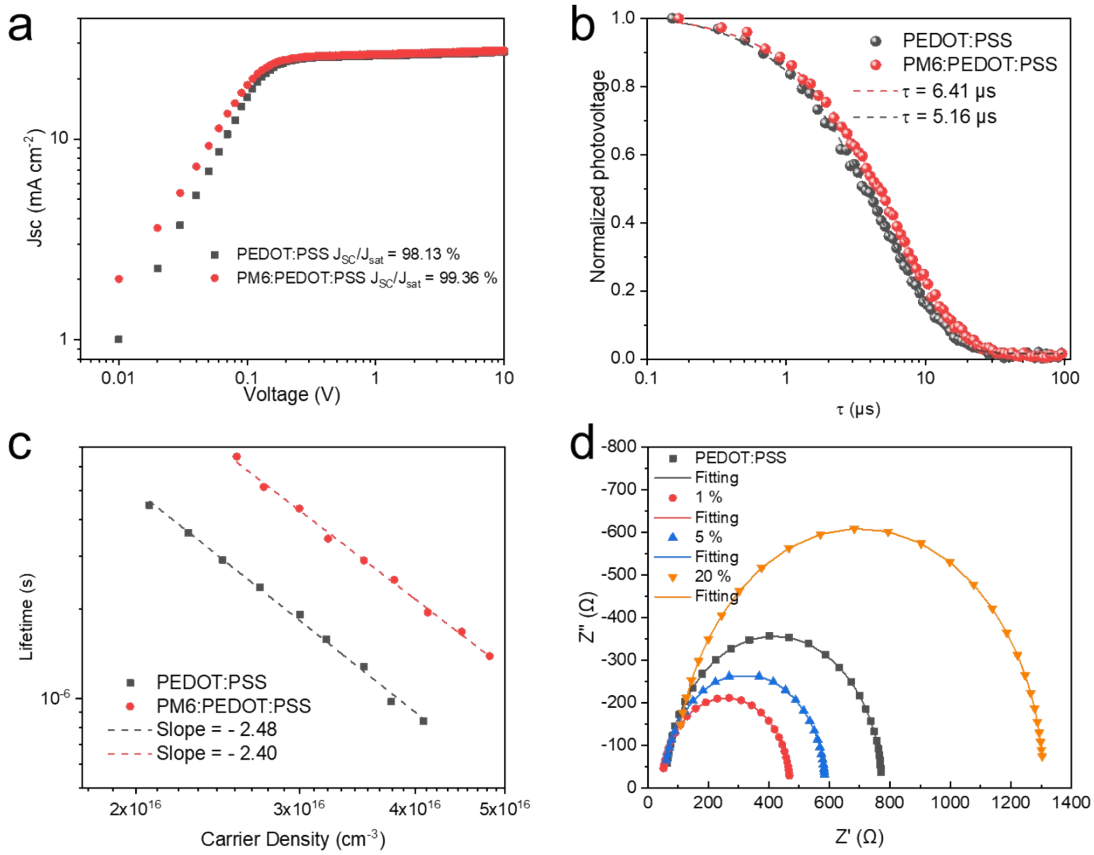

Figure S18. (a) Photocurrent, (b) TPV spectra, TPV-CE and (d) Nyquist plots of PM6:L8-BO devices with PEDOT:PSS and PM6:PEDOT:PSS as HTLs.

Table S6. Summary of calculated device physics parameters of PM6:L8-BO-based binary OSCs with different HTLs.

HTL	J_{SC}/J_{sat}[a] (%)	μ[b] (cm^2 $V^{-1}s^{-1}$)	τ[c] (μs)	t_S[d] (μs)	K_{rec}[e] (cm^3 s^{-1})	n[f] (cm^{-3})
PEDOT:PSS	98.13	1.64×10^{-4}	6.41	0.35	8.39×10^{-12}	4.09×10^{16}
PM6 (10%) :PEDOT:PSS	99.36	2.09×10^{-4}	5.16	0.27	4.42×10^{-12}	4.81×10^{16}

[a] The ratio between Jsc and saturate current density from photocurrent measurements. [b] Carrier mobility values from phto-CELIV measurements. [c] Charge carrier lifetime from TPV measurement, [d] sweeping out time from TPC measurement. [e] Bimolecular recombination rate constant. [f] Charge carrier density.

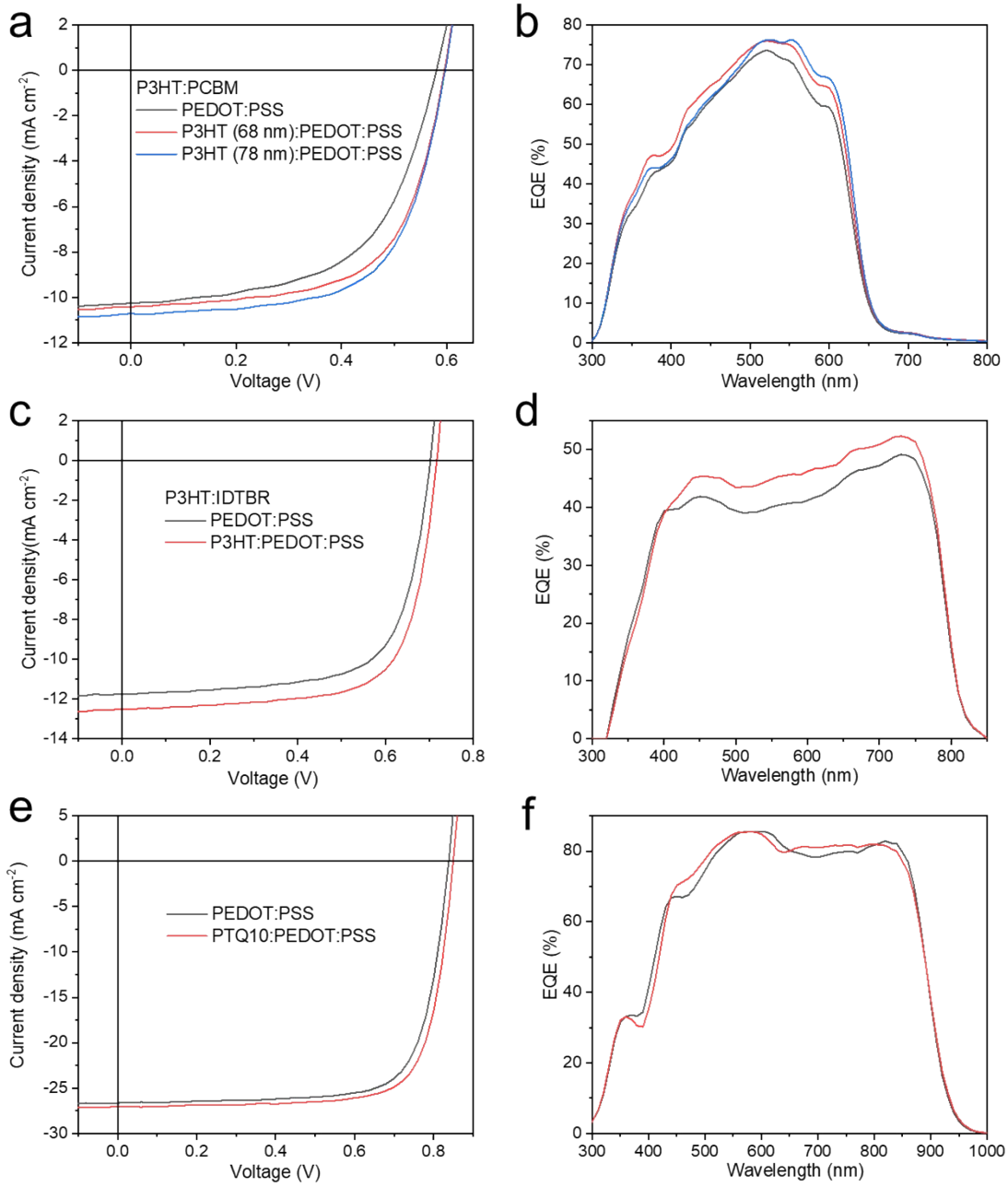

Figure S19. J-V curves and EQE spectra of (a,b) P3HT:PCBM, (c,d) P3HT:IDTBR and (e,f) PTQ10:Y6 solar cells with different HTLs.

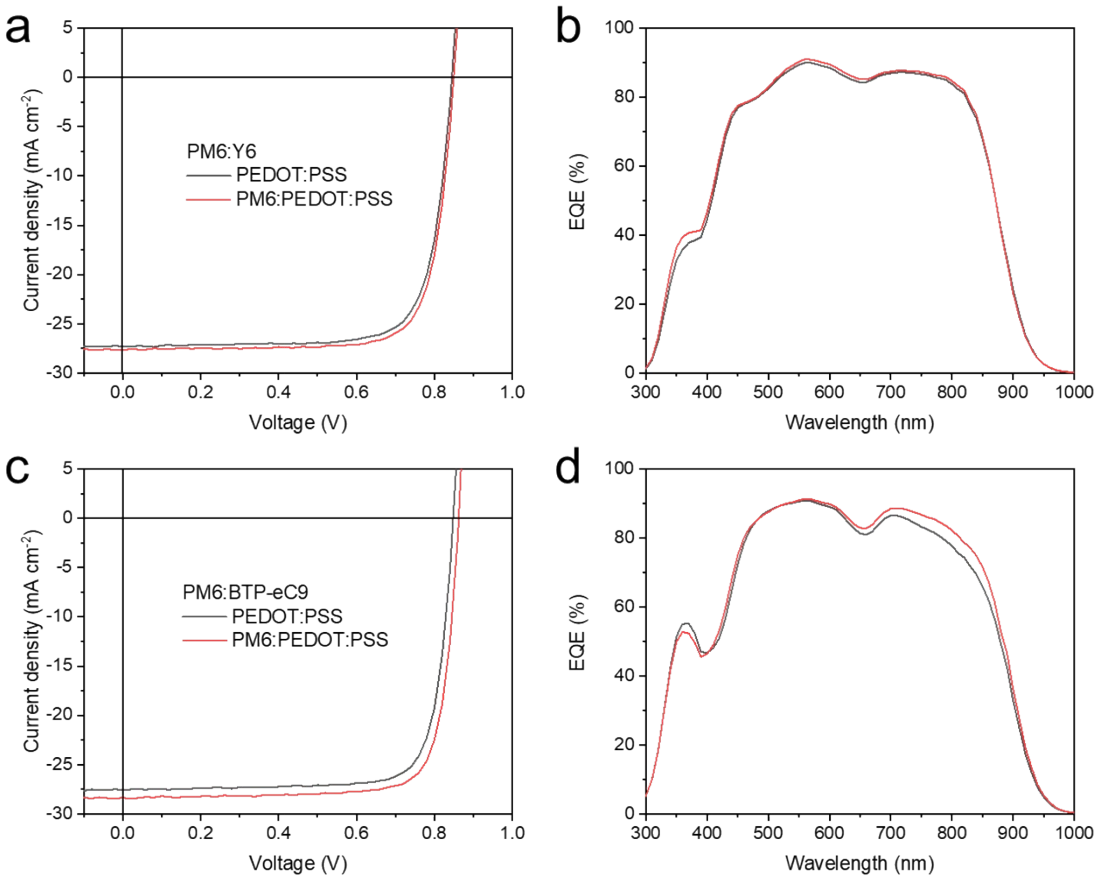

Figure S20. J-V curves and EQE spectra of (a,b) PM6:Y6 and (c,d) PM6:BTP-eC9 solar cells with different HTLs.

Table S7. Summary of photovoltaic parameters of solar cells with different active layer materials and HTLs.

Active layer	HTL	V_{OC} (V)	J_{SC} (mA cm^{-2})	J_{SC}[b] (mA cm^{-2})	FF (%)	PCE[c] (%)
P3HT:PCBM	PEDOT:PSS	0.580	10.26	9.78	55.66	3.31 (3.04 ± 0.27)
	P3HT (77 nm):PEDOT:PSS[a]	0.595	10.57	10.49	63.44	3.99 (3.83 ± 0.16)
	P3HT (68 nm):PEDOT:PSS[a]	0.594	10.25	10.45	62.49	3.80 (3.65 ± 0.15)
P3HT:IDTBR	PEDOT:PSS	0.701	11.79	11.13	68.01	5.62 (5.52 ± 0.10)
	P3HT (77 nm): PEDOT:PSS[a]	0.715	12.55	12.31	69.63	6.25 (6.10 ± 0.15)
PTQ10:Y6	PEDOT:PSS	0.837	26.35	25.57	74.91	16.51 (16.40 ± 0.20)
	PTQ10 (81 nm): PEDOT:PSS[a]	0.848	26.75	25.89	75.95	17.22 (17.05 ± 0.17)
PM6:Y6	PEDOT:PSS	0.842	27.28	26.53	77.16	17.60 (17.32 ± 0.28)
	PM6 (65 nm): PEDOT:PSS[a]	0.847	27.42	26.79	78.02	18.13 (17.95 ± 0.18)
PM6:BTP-eC9	PEDOT:PSS	0.845	27.58	26.59	79.10	18.44 (18.30 ± 0.14)
	PM6 (65 nm): PEDOT:PSS[a]	0.859	28.35	27.34	79.50	19.36 (19.10 ± 0.26)

[a] All the target HTLs with 1% donor;

[b] Calculated from EQE;

[c] Average values with standard deviation were obtained from 20 devices;

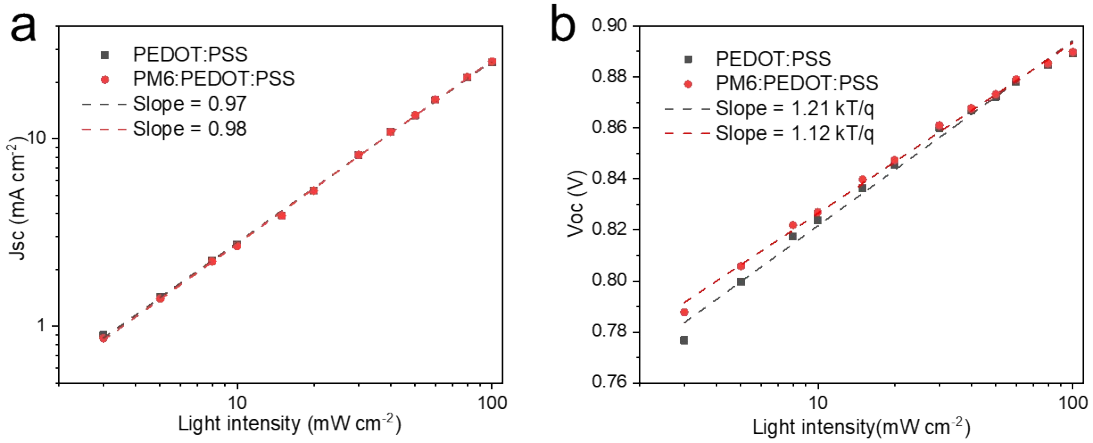

Figure S21. (a) Jsc and (b) Voc as a function of light intensity of PM6:L8-BO devices processed by PEDOT:PSS and PM6:PEDOT:PSS.

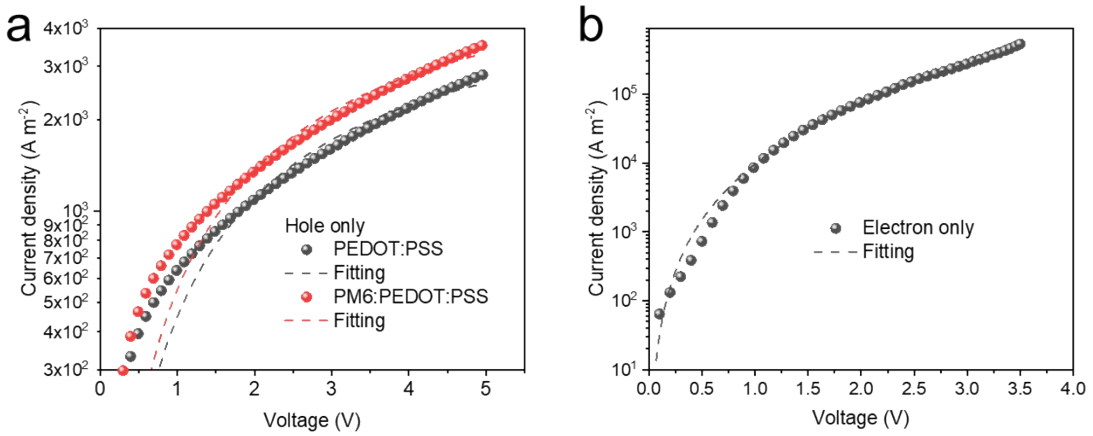

Figure S22. Dark J-V curves of electron only PM6:L8-BO devices.

Table S8. Fitting hole and electron mobilities from SCLC measurements.

PM6 percentage in HTL	μ_h ($\times10^{-4}$ cm^2 V^{-1} s^{-1})	μ_e ($\times10^{-4}$ cm^2 V^{-1} s^{-1})	μ_h/μ_e
0%	4.82	6.39	0.754
1%	5.83		0.912
5%	4.73		0.740
20%	1.50		0.235

Table S9. Fitting parameters for OPVs from Nyquist plots.

PM6 percentage in HTL	Rs (Ω)	Rp (Ω)	C_1 (nF)
0%	59.44	713.6	14.47
1%	46.46	423.3	7.23
5%	53.26	533	7.34
20%	89.37	1218	8.38

Table S10. Calculated dielectric parameters of PM6:L8-BO devices with different HTLs.

HTL	V_{bi} (V)	C_{1kHZ} (nF)	ε_r	Nt (10^{15} cm^{-3})
PEDOT:PSS	0.790	2.43	2.75	9.38
PM6:PEDOT:PSS	0.815	2.46	2.78	9.19

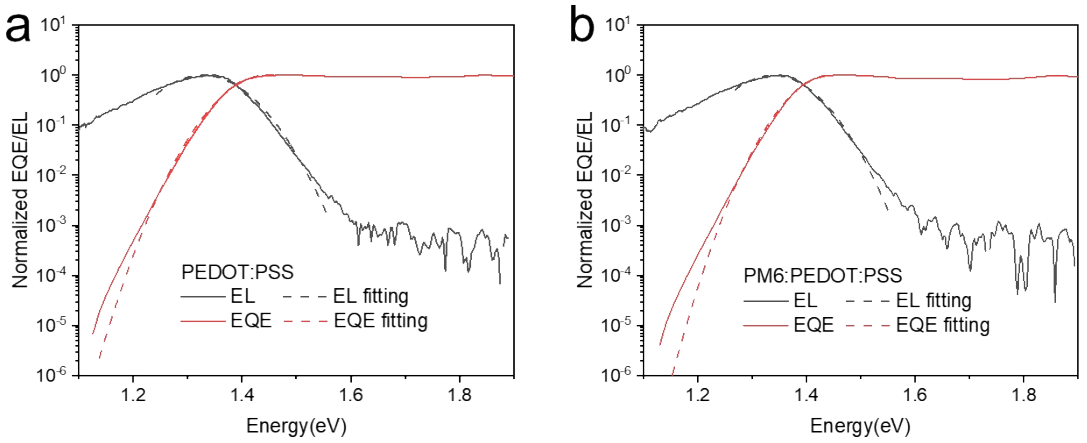

Figure S23. FTPS-EQE and EL spectra of PM6:L8-BO devices with (a) PEDOT:PSS and (b) PM6:PEDOT:PSS as HTLs.

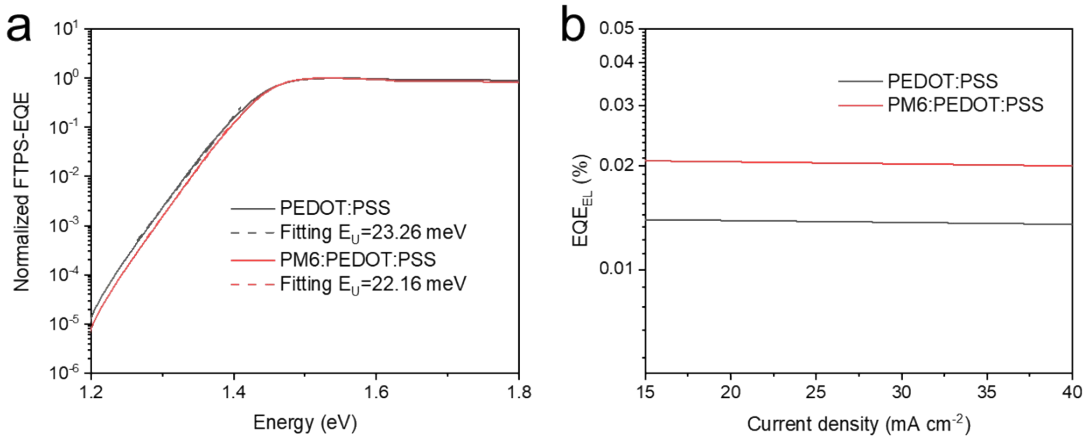

Figure S24. (a) FTPS-EQE and (b) EQE_{EL} of PM6:L8-BO devices. E_U is Urbach energy, which is obtained from the FTPS-EQE curves with the exponential fitting $\{E_u = A \cdot \exp[(E-E_g)/E_u]\}$.

Table S11. Summary of energy loss data of PM6:L8-BO devices with different HTL

HTL	Eg (eV)	$qV_{OC,SQ}$ (eV)	$qV_{OC,Rad}$ (eV)	EQE_{EL} ($\times10^{-4}$)	ΔE_1 (eV)	ΔE_2 (eV)	ΔE_3 (eV)	E_{loss} (eV)
PEDOT:PSS	1.446	1.182	1.126	1.391	0.264	0.056	0.230	0.550
PM6:PEDOT:PSS	1.449	1.184	1.130	2.035	0.265	0.054	0.221	0.540

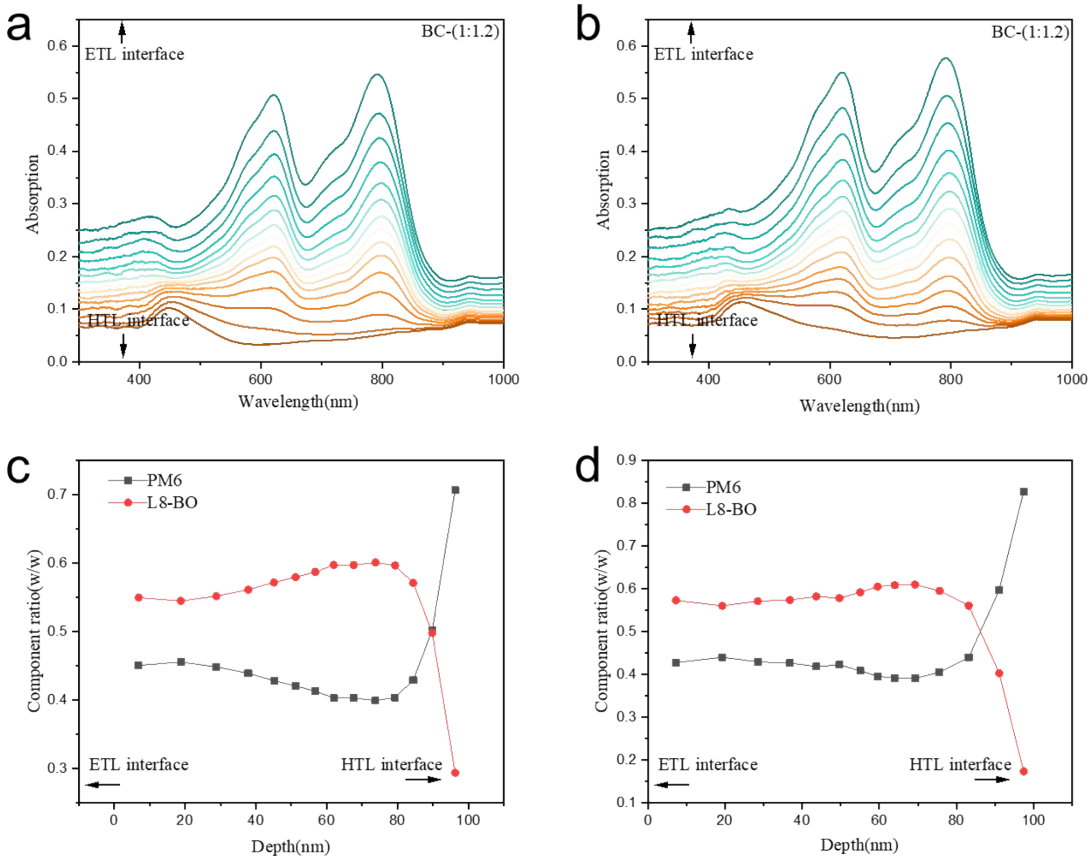

Figure S25. Layered absorption spectra of PM6:L8-BO devices with (a) PEODT and (c) PM6:PEDOT:PSS as HTLs from FLAS measurement. Composition ratio in the vertical direction of the active layer film with (c) PEODT and (d) PM6 (1%) :PEDOT:PSS as HTLs.

Table S12. The peak positions, d-spacings, FWHMs and CCLs of PM6:L8-BO films processed on different HTLs with PM6 NP.

PM6 percentage in HTL	IP				OOP			
	q ($Å^{-1}$)	d-spacing(Å)	FWHM ($Å^{-1}$)	CCL(Å)	q ($Å^{-1}$)	d-spacing (Å)	FWHM ($Å^{-1}$)	CCL (Å)
0	0.302	20.80	0.092	61.19	1.662	3.780	0.343	16.47
1%	0.302	20.80	0.083	68.54	1.662	3.780	0.319	17.74
5%	0.302	20.80	0.085	66.50	1.662	3.780	0.351	16.11
0 aged	0.297	21.12	0.038	14.94	1.708	3.678	0.984	5.75
1% aged	0.297	21.12	0.367	15.41	1.681	3.738	0.724	7.81
5% aged	0.297	21.12	0.358	15.79	1.662	3.780	0.858	6.59

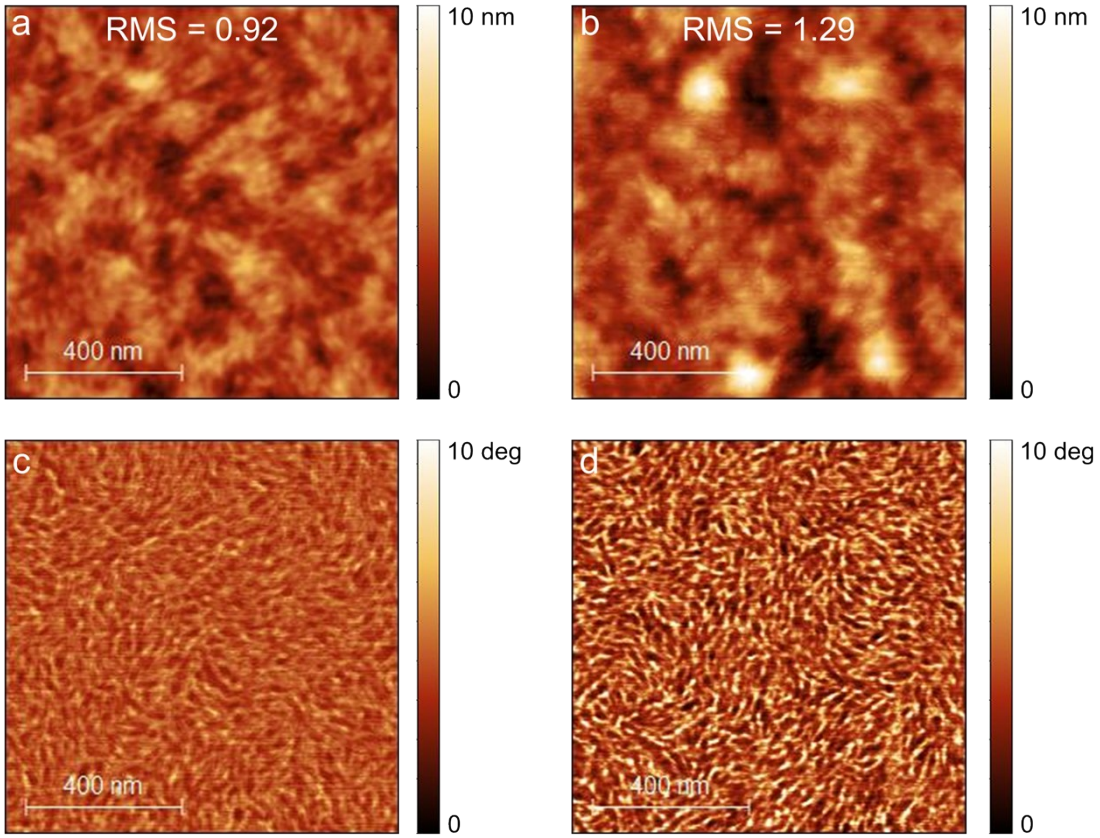

Figure S26. AFM (a,b) height and (c,d) phase images of PM6:L8-BO film on top of (a,c) PEDOT:PSS and (b,d) PM6 (1%):PEDOT:PSS.

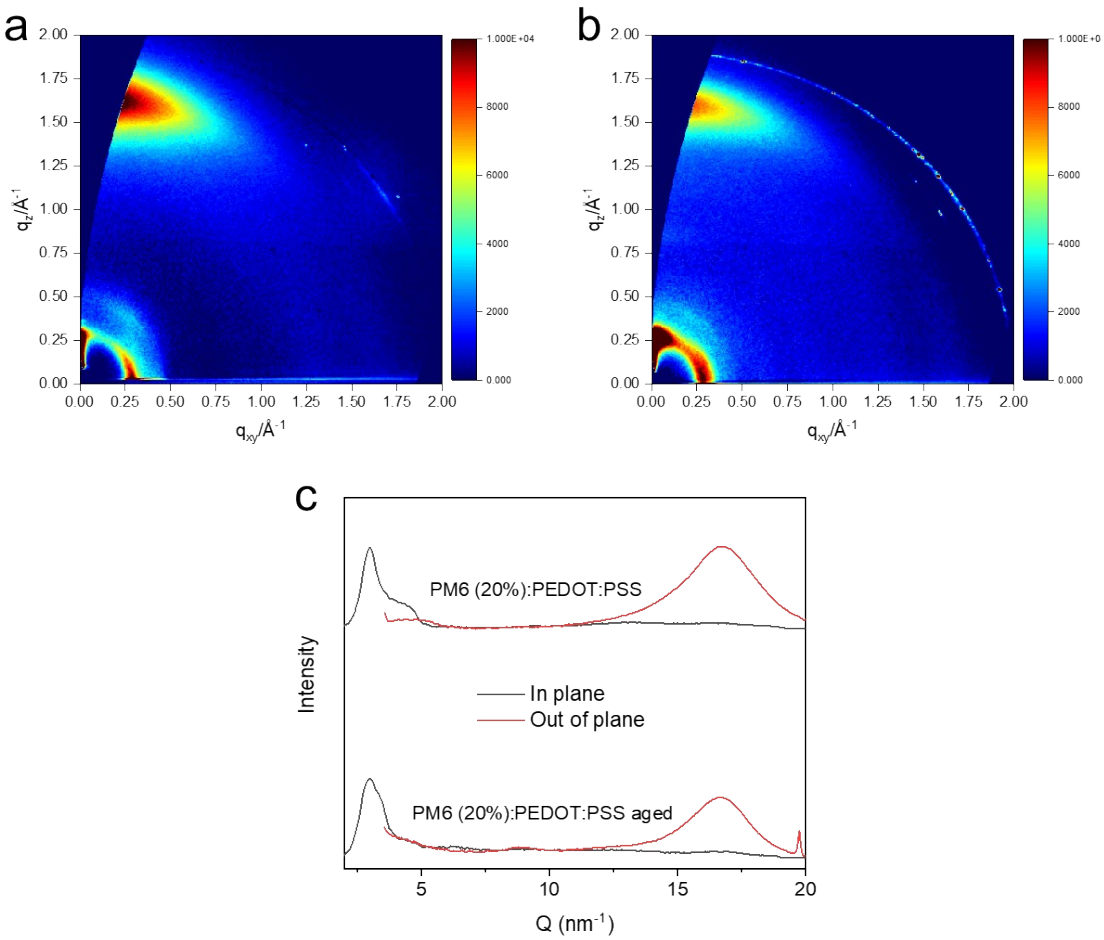

Figure S27. 2D GIWAXS patterns of PM6:L8-BO film on PM6 (20%):PEDOT:PSS (a) before and (b) after continuous illumination for 4 weeks as well as (c) their corresponding in-plane and out-of-plane line-cuts.

References

1 P. W. M. Blom, M. J. M. De Jong and J. J. M. Vleggaar, *Appl. Phys. Lett.*, 1996, **68**, 3308–3310.

2 C. Xie, A. Classen, A. Späth, X. Tang, J. Min, M. Meyer, C. Zhang, N. Li, A. Osvet, R. H. Fink and C. J. Brabec, *Adv. Energy Mater.*, 2018, **8**, 1702857.

3 T. Schiros, G. Kladnik, D. Prezzi, A. Ferretti, G. Olivieri, A. Cossaro, L. Floreano, A. Verdini, C. Schenck, M. Cox, A. A. Gorodetsky, K. Plunkett, D. Delongchamp, C. Nuckolls, A. Morgante, D. Cvetko and I. Kymissis, *Adv. Energy Mater.*, 2013, **3**, 894–902.

4 C. Zhan, X. Zhang and J. Yao, *RSC Adv.*, 2015, **5**, 93002–93026.

5 Y. Zhang, D. Deng, Z. Wang, Y. Wang, J. Zhang, J. Fang, Y. Yang, G. Lu, W. Ma and Z. Wei, *Adv. Energy Mater.*, 2017, **7**, 1701548.

6 L. Bu, S. Gao, W. Wang, L. Zhou, S. Feng, X. Chen, D. Yu, S. Li and G. Lu, *Adv. Electron. Mater.*, 2016, **2**, 1600359.

7 X. Feng, Y. Wang, T. Xiao, Z. Shen, Y. Ren, G. Lu and L. Bu, *Front. Chem.*, 2020, **8**, 1–10.

8 Z. Zhou, W. Liu, G. Zhou, M. Zhang, D. Qian, J. Zhang, S. Chen, S. Xu, C. Yang, F. Gao, H. Zhu, F. Liu and X. Zhu, *Adv. Mater.*, 2020, **32**, 1–8.

9 L. Liu, Y. Kan, K. Gao, J. Wang, M. Zhao, H. Chen, C. Zhao, T. Jiu, A. K. Y. Jen and Y. Li, *Adv. Mater.*, 2020, **32**, 1907604.

10 Y. Cui, H. Yao, J. Zhang, K. Xian, T. Zhang, L. Hong, Y. Wang, Y. Xu, K. Ma, C. An, C. He, Z. Wei, F. Gao and J. Hou, *Adv. Mater.*, 2020, **32**, 1908205.

11 J. Yao, B. Qiu, Z. G. Zhang, L. Xue, R. Wang, C. Zhang, S. Chen, Q. Zhou, C. Sun, C. Yang, M. Xiao, L. Meng and Y. Li, *Nat. Commun.*, 2020, **11**, 1–10.

12 C. Li, J. Zhou, J. Song, J. Xu, H. Zhang, X. Zhang, J. Guo, L. Zhu, D. Wei, G. Han, J. Min, Y. Zhang, Z. Xie, Y. Yi, H. Yan, F. Gao, F. Liu and Y. Sun, *Nat. Energy*, 2021, **6**, 605–613.

13 L. Hong, H. Yao, Y. Cui, P. Bi, T. Zhang, Y. Cheng, Y. Zu, J. Qin, R. Yu, Z. Ge and J. Hou, *Adv. Mater.*, 2021, **33**, 1–8.

14 C. He, Y. Pan, G. Lu, B. Wu, X. Xia, C. Q. Ma, Z. Chen, H. Zhu, X. Lu, W.

Ma, L. Zuo and H. Chen, *Adv. Mater.*, 2022, **34**, 1–10.

15 Y. Wei, Z. Chen, G. Lu, N. Yu, C. Li, J. Gao, X. Gu, X. Hao, G. Lu, Z. Tang, J. Zhang, Z. Wei, X. Zhang and H. Huang, *Adv. Mater.*, 2022, **34**, 2204718.

16 C. Li, X. Gu, Z. Chen, X. Han, N. Yu, Y. Wei, J. Gao, H. Chen, M. Zhang, A. Wang, J. Zhang, Z. Wei, Q. Peng, Z. Tang, X. Hao, X. Zhang and H. Huang, *J. Am. Chem. Soc.*, 2022, **144**, 14731–14739.

17 M. Zhou, C. Liao, Y. Duan, X. Xu, L. Yu, R. Li and Q. Peng, *Adv. Mater.*, 2023, **35**, 1–11.

18 J. Wang, Y. Wang, P. Bi, Z. Chen, J. Qiao and J. Li, 2023, **2301583**, 1–11.

19 J. Fu, P. W. K. Fong, H. Liu, C. Huang, X. Lu, S. Lu, M. Abdelsamie, T. Kodalle, C. M. Sutter-fella, Y. Yang and G. Li, , DOI:10.1038/s41467-023-37526-5.

20 L. Wang, C. Chen, Y. Fu, C. Guo, D. Li, J. Cheng, W. Sun, Z. Gan, Y. Sun, B. Zhou, C. Liu, D. Liu, W. Li and T. Wang, *Nat. Energy*, 2024, **9**, 208–218.

21 S. Chen, S. Zhu, L. Hong, W. Deng, Y. Zhang, Y. Fu, Z. Zhong, M. Dong, C. Liu, X. Lu, K. Zhang and F. Huang, *Angew. Chemie - Int. Ed.*, , DOI:10.1002/anie.202318756.

22 R. Xu, Y. Jiang, F. Liu, G. Ran, K. Liu, W. Zhang and X. Zhu, *Adv. Mater.*, 2024, **36**, 2312101.

23 K. Liu, Y. Jiang, K. Liu, Y. Jiang, G. Ran, F. Liu and W. Zhang, *Joule*, 2024, 1–17.